



# HHS Public Access

Author manuscript

*J Biomech.* Author manuscript; available in PMC 2018 May 03.

Published in final edited form as:

*J Biomech.* 2017 May 03; 56: 102–110. doi:10.1016/j.jbiomech.2017.03.012.

## A Four-Dimensional Computed Tomography Comparison of Healthy vs. Asthmatic Human Lungs

Nariman Jahani<sup>1,2,3</sup>, Sanghun Choi<sup>1,4</sup>, Jiwoong Choi<sup>1,2</sup>, Babak Haghghi<sup>1,2</sup>, Eric A. Hoffman<sup>5,6,7</sup>, Alejandro P. Comellas<sup>6</sup>, Joel N. Kline<sup>6</sup>, and Ching-Long Lin<sup>1,2,\*</sup>

<sup>1</sup>Department of Mechanical and Industrial Engineering, The University of Iowa, Iowa City, IA, USA

<sup>2</sup>IHR-Hydroscience & Engineering, The University of Iowa, Iowa City, IA, USA

<sup>3</sup>Department of Radiology, University of Pennsylvania Perelman School of Medicine, Philadelphia, PA, USA

<sup>4</sup>Department of Mechanical Engineering, Kyungpook National University, Daegu, South Korea

<sup>5</sup>Department of Biomedical Engineering, The University of Iowa, Iowa City, IA, USA

<sup>6</sup>Department of Internal Medicine, The University of Iowa, Iowa City, IA, USA

<sup>7</sup>Department of Radiology, The University of Iowa, Iowa City, IA, USA

### Abstract

The purpose of this study was to explore new insights in non-linearity, hysteresis and ventilation heterogeneity of asthmatic human lungs using four-dimensional computed tomography (4D-CT) image data acquired during tidal breathing. Volumetric image data were acquired for 5 non-severe and one severe asthmatic volunteers. Besides 4D-CT image data, function residual capacity and total lung capacity image data during breath-hold were acquired for comparison with dynamic scans. Quantitative results were compared with the previously reported analysis of five healthy human lungs. Using an image registration technique, local variables such as regional ventilation and anisotropic deformation index (ADI) were estimated. Regional ventilation characteristics of non-severe asthmatic subjects were similar to those of healthy subjects, but different from the severe asthmatic subject. Lobar airflow fractions were also well correlated between static and dynamic scans ( $R^2 > 0.84$ ). However, local ventilation heterogeneity significantly increased during tidal breathing in both healthy and asthmatic subjects relative to that of breath-hold perhaps because of airway resistance present only in dynamic breathing. ADI was used to quantify non-linearity and hysteresis of lung motion during tidal breathing. Nonlinearity was greater on inhalation than exhalation among all subjects. However, exhalation nonlinearity among asthmatic

\*Corresponding author: Ching-Long Lin, Address: 2406 Seamans Center for the Engineering Arts and Science, Iowa City, Iowa, 52242, USA, Tel: +1 319 335 5673, fax: 319-335-5669, ching-long-lin@uiowa.edu.

#### Conflicts of Interest Statement

There is no conflict of interest although E. A. Hoffman is a founder and shareholder of VIDA Diagnostics, a company commercializing lung image analysis software developed, in part, at the University of Iowa. He is also a member of the Siemens CT advisory board.

**Publisher's Disclaimer:** This is a PDF file of an unedited manuscript that has been accepted for publication. As a service to our customers we are providing this early version of the manuscript. The manuscript will undergo copyediting, typesetting, and review of the resulting proof before it is published in its final citable form. Please note that during the production process errors may be discovered which could affect the content, and all legal disclaimers that apply to the journal pertain.

subjects was greater than healthy subjects and the difference diminished during inhalation. An increase of non-linearity during exhalation in asthmatic subjects accounted for lower hysteresis relative to that of healthy ones. Thus, assessment of nonlinearity differences between healthy and asthmatic lungs during exhalation may provide quantitative metrics for subject identification and outcome assessment of new interventions.

## Keywords

four-dimensional computed tomography; asthma; ventilation heterogeneity; hysteresis; image registration

## 1. Introduction

In obstructive lung diseases, such as asthma, accurate quantification of regional features and their heterogeneity is essential for advancing our understanding of the underlying mechanisms of disease. Due to non-linear behavior and hysteresis of lung motion, the analysis for breathing lungs is desirable to characterize alterations of regional ventilation and tissue deformation in asthmatic lungs. Magnetic resonance (MR) imaging (Campana et al., 2009; de Lange et al., 2006), single-photon emission computed tomography (SPECT) (King et al., 1997; King et al., 2010) and X-ray computed tomography (CT) (Chae et al., 2010) have recently been used to advance understanding of the lung function in asthmatic patient, but imaging has been carried out during inspiratory and expiratory breath-holds. Using those static breath-hold techniques, regional analysis has been performed to identify the regions of airflow obstruction and airway resistance in asthmatics (Choi et al., 2013; de Lange et al., 2007). However, it is well recognized that hysteresis, representative of regional differences in lung mechanics, is minimized or eliminated during step-wise inflation or deflation of the lung. Although MR imaging and SPECT have advantages that they are non-invasive and SPECT can provide information related to both perfusion and ventilation simultaneously, these imaging modalities have limitation in analysis of lung functions due to their long scanning time and higher cost especially during dynamic breathing (Chang et al., 1987). With the introduction of four-dimensional CT (4D-CT) methods for assessing lungs under well controlled tidal breathing (Jahani et al., 2015) and with the introduction of ultra low-dose CT imaging methods which maintain quantitative accuracy of the reconstructed image (Newell et al., 2015), dynamic imaging for total lung volume is feasible during active respiration. Advances in image registration techniques provide the ability to assess regional functional and structural metrics such as ventilation and directional tissue deformation (Jahani et al., 2014; Reinhardt et al., 2008; Yin et al., 2009).

Jahani et al., (2015) have utilized 4D-CT image data for healthy human lungs to estimate regional ventilation and hysteresis of lung motion. The study demonstrated that non-linearity was greater in lower regions and it was smaller during exhalation. Although some studies have applied 4D-CT imaging in patients with emphysema (Yamamoto et al., 2011) and lung cancers (Boldea et al., 2008; White et al., 2013), it has yet to be investigated for asthmatics. In a study of healthy vs. asthmatic lungs, with matching of breath-hold scans, Choi et al., (2014) showed similar lung function for healthy and non-severe asthmatic lungs by

estimating ventilation and air trapping. In a different study, they quantified structural and functional alterations for non-severe and severe asthmatics, yet the alterations in non-severe asthmatics were not significant as compared with severe asthmatics (Choi et al., 2015). It is our hypothesis that because of airway resistance, dynamic imaging will serve to enhance the heterogeneity of lung function metrics. Furthermore, it is expected analysis of dynamic imaging provide new information about lung deformation in asthmatics which can be extracted by quantifying non-linearity and hysteresis of lung motion.

This study aims to assess regional ventilation and deformation for asthmatic human lungs using 4D-CT technique for comparison with our already reported healthy population (Jahani et al., 2015). We utilize a unique dual rolling-seal piston to control tidal breathing for consistent reconstruction of lung volumes (Fuld et al., 2012; Jahani et al., 2015). In addition, a mass preserving image registration (Yin et al., 2009) is employed to derive regional ventilation and anisotropic deformation. In this study, ventilation heterogeneity estimated from dynamic images of healthy and asthmatic subjects are compared with those obtained from static deep-breathing images. We seek to establish tools for assessing heterogeneity, for the development and assessment of new interventions and to better sub-phenotype an asthma population. In addition, precise estimation of regional ventilation during breathing can provide physiological boundary conditions for computational fluid dynamic (CFD) analysis in quantifying airflow and pressure distribution (Yin et al., 2010; Yin et al., 2013). Furthermore, anisotropic deformation is utilized to quantify non-linearity and hysteresis of lung motion for healthy vs. asthmatic lungs. A motivation for quantification of non-linearity and hysteresis is to capture abnormal movements and sensitive regions regarding to motion within asthmatic lungs.

## 2. Method

### 2.1. Image Data acquisition

Datasets were acquired from 5 non-severe asthmatics and one severe asthmatic volunteers for comparison with previously acquired set of 5 healthy subjects (Jahani et al., 2015). A full set of pulmonary function tests (PFTs) were performed in upright body posture. The PFTs provided preliminary information such as total lung capacity (TLC), functional residual capacity (FRC), residual volume (RV), vital capacity (VC), forced vital capacity (FVC), and forced expiratory volume in 1 second (FEV1). Asthmatics and their severity were categorized based on National Heart Lung and Blood Institute (2007) guidelines for the diagnosis and management of asthma.

CT scanning was performed to acquire static and dynamic MDCT images in supine position, withholding of bronchodilators for 12 hours to observe baseline lung function. Static scans were acquired approximately at FRC (~15% VC) and TLC (95% VC) using a pneumotachometer-controlled device to achieve accurate breath-hold volumes (Iyer et al., 2014). For dynamic imaging, a dual rolling-seal piston system (Fuld et al., 2012) was utilized to control amplitudes of inhalation and exhalation during breathing as previously described (Jahani et al., 2015). Reconstruction of volumetric image was performed at 10–14 selected phases of each subject's respiratory cycle.

All subjects were studied under the University of Iowa Institutional Review Board and the radiation safety committee approval and with informed consent. Siemens Somatom Definition Flash dual-source 128-slice MDCT scanner (Forchheim, Germany) was utilized for the scanning. The parameters for scanner such as scan type, slice thickness, peak voltage and effective current were set to spiral, 0.75 mm, 120 kV and 75 mAs, respectively. All images were acquired at a reconstruction matrix of  $512 \times 512$  and a section spacing of 0.5 mm with use of B35f kernel. Furthermore, to segment lungs for every volumetric image, a semi-automatic segmentation software, Apollo (VIDA Diagnostics, Coralville, Iowa), was employed in the same way as for the prior healthy volunteers (Jahani et al., 2015).

## 2.2. Single respiratory cycle

The lung volume in each phase was achieved by reconstructing multi-slices acquired from several respiratory cycles. To construct a single respiratory cycle, air volumes and corresponding times, recorded by a turbine-based flow meter, were normalized at the  $n^{\text{th}}$  cycle ( $V_{air}^{*n}$  and  $t^{*n}$ , respectively). The mean of those normalized air volumes for all cycles was obtained for a single respiratory cycle and was denoted by  $V_{air}^*(t^*)$  at each normalized time  $t^*$  where  $0 \leq t^* \leq 1$ . Thus,  $V_{air}^*$  is normalized air volume defined as  $(V_{air} - V_{air,EE}) / (V_{air,EI} - V_{air,EE})$  where  $V_{air}$  is total air volume in each phase (EE: end exhalation; EI: end inhalation), for more details, see Jahani et al., (2015). Thus, the normalized total airflow  $Q^*$  at time point  $t_p^*$  was computed as:

$$Q^*(t_p^*) = \left( \frac{dV_{air}^*}{dt^*} \right)_{t_p^*} \approx \frac{V_{air}^*(t_{p+1/2}^*) - V_{air}^*(t_{p-1/2}^*)}{t_{p+1/2}^* - t_{p-1/2}^*}. \quad (1)$$

The time step ( $t_{p+1/2}^* - t_{p-1/2}^*$ ) was set to 0.01.

## 2.3. Image Registration

We extracted fractions of lung tissue and air volume using CT density in Hounsfield Unit (HU) as:

$$\beta_{tissue}(\mathbf{x}) = \frac{I(\mathbf{x}) - HU_{air}}{HU_{tissue} - HU_{air}}, \text{ and } \beta_{air}(\mathbf{x}) = \frac{HU_{tissue} - I(\mathbf{x})}{HU_{tissue} - HU_{air}}, \quad (2)$$

where  $\beta_{tissue}(\mathbf{x})$ ,  $\beta_{air}(\mathbf{x})$ ,  $I(\mathbf{x})$ ,  $HU_{tissue}$  and  $HU_{air}$  are tissue fraction, air fraction, image density at position  $\mathbf{x}$ , HU of tissue and HU of air, respectively. We set 55 for  $HU_{tissue}$  and -1000 for  $HU_{air}$ .

A mass preserving registration method (Yin et al., 2009) was utilized to obtain a spatial transformation  $\mathbf{T}(\mathbf{x})$  to match each pair of images at differing inflation levels. A free form deformation (FFD) interpolated by cubic B-spline functions was applied to estimate motion of each voxel. One image was considered as a reference image, and the other was considered as a moving image. To preserve local tissue volumes, we minimized a similarity function (E) defined based on the sum of squared tissue volume difference (SSTVD), as:

$$E = \sum_{x \in \Omega} [v_r(\mathbf{x})\beta_{tissue,r}(\mathbf{x}) - v_m(T(\mathbf{x}))\beta_{tissue,m}(T(\mathbf{x}))]^2 \quad (3)$$

where  $v$  is local volume in each voxel and subscripts  $r$  and  $m$  are for reference and moving volumes, respectively. For dynamic images at time points in the respiratory cycle, the lung image at the EE was adopted as the reference for registration. For the registration between static scans the image at TLC was taken as the reference.

#### 2.4. Registration-derived variables

Local air volume,  $v_{air}$  at location  $\mathbf{x}$  was computed with  $\mathbf{T}(\mathbf{x})$  as

$$v_{air}(\mathbf{x}) = v(\mathbf{T}(\mathbf{x}))\beta_{air}(\mathbf{T}(\mathbf{x})). \quad (4)$$

With Eq. 4, regional air volume fraction,  $v_{f,air}$  was defined as the ratio of sum of  $v_{air}$  in each region (voxels or lobes) to total air volume. Furthermore, for consistency with air volume measured by the turbine-based flow meter, normalized local air volume ( $v_{air}^*$ ) during tidal breathing was calculated as:

$$v_{air}^* = \frac{v_{air} - v_{air,EE}}{V_{air,EI} - V_{air,EE}}, \quad (5)$$

where  $V_{air,EI}$  (or  $V_{air,EE}$ ) is the sum of local air volumes at EI (or EE) within the whole lung.

Furthermore, air trapping percentage (AirT%) was defined as the ratio of number of voxels with air trapping to total number of voxels in each lobe or total lung. Instead of single density-threshold-based air trapping approach ( $I_{threshold} = -850$  HU) (Busacker et al., 2009), we used a fraction-threshold-based approach ( $\beta_{air,threshold} = 0.9$ ) to eliminate inter-subject variability (Choi et al., 2014). The subject-specific threshold ( $I_{threshold}$ ) is calculated as

$$I_{threshold} = (1 - \beta_{air,threshold})HU_{tissue} + \beta_{air,threshold}HU_{air,trachea} \quad (6)$$

where  $HU_{air,trachea}$  is the median of CT density of air extracted from tracheal region. To derive  $HU_{air,trachea}$ , we first extracted airway masks using Apollo pulmonary analysis software, and consistently eroded the airway masks with a ball-shaped element of radius of six voxels for the purpose of excluding partially contaminated voxels.

We then assessed local anisotropic deformation using principle strains, i.e.,  $\lambda_1 > \lambda_2 > \lambda_3$ , obtained from lung displacement field (Amelon et al., 2011). The anisotropic deformation index (ADI) was calculated as

$$ADI = \sqrt{\left(\frac{\lambda_1 - \lambda_2}{\lambda_2}\right)^2 + \left(\frac{\lambda_2 - \lambda_3}{\lambda_3}\right)^2} \quad (7)$$

ADI quantified the degree of preferential deformation of a local volume. We normalized ADI with its value at EI ( $ADI^*$ ). Non-linearity,  $\delta_{ADI^*}$ , at each location was defined as the deviation of the  $ADI^*$  curve from identity line between EE and EI. In addition, the hysteresis,  $Hys_{ADI^*}$  was quantified by the absolute difference between the  $ADI^*$  of inhalation and exhalation at the same normalized total air volumes  $V_{air}^*$ .

## 2.5. Interpolation method

A cubic spline interpolation was utilized to estimate a continuous function for each variable. The interpolated values at phase  $i$  were computed from the values derived from given lung images as a function of  $V_{air}^* [s_i(V_{air}^*)]$  (Jahani et al., 2015), where  $s_i$  is a local variable interpolated in the interval of ( $V_{air,i}^*, V_{air,i+1}^*$ ). The variable  $s$  was either  $v_{air}^*$  or  $ADI^*$ . Thus, the local normalized airflow ( $\frac{dv_{air}^*}{dt^*}$ ) was calculated as  $\frac{dv_{air}^*}{dV_{air}^*} \left(\frac{dV_{air}^*}{dt^*}\right)$  by chain rule from the composition of the derivative of  $v_{air}^*$  and the derivative of breathing waveform (Eq. 1). Consequently, the local airflow fraction ( $q_f$ ) was computed as the ratio of local airflow to total airflow:

$$q_f = \frac{dv_{air}^*}{dV_{air}^*} \quad (8)$$

To compare air volume change between static and dynamic scans, we assumed linear interpolation between TLC and FRC and the average values from cubic interpolation between EE and EI, respectively. For linear assumption,  $q_f$  was simplified as the ratio of local air volume change to total air volume change ( $v_{air}/V_{air}$ ). Furthermore, regional coefficient of variations (CV) of air volume changes (defined as standard deviation of  $v_{air}/V_{air}$  mean of  $v_{air}$  in total lung or in each lobe) was calculated to quantify heterogeneity.

## 3. Results

### 3.1. PFT-, CT-based volumes, and air-trapping percentage

Table 1 indicated demographic information and PFT, %predicted values, (Stocks and Quanjer, 1995; Hankinson et al., 2010; Hankinson et al., 1999) of five healthy, five non-severe, and one severe asthmatic subjects. FEV1, %predicted values and FEV1/FVC for non-severe asthmatic subjects were significantly smaller than those of healthy subjects ( $P < 0.01$ ). FRC and RV, %predicted values of non-severe asthmatics were within normal range while those of the severe asthmatic subject were greater than normal range. Furthermore, TLC and FRC values obtained from CT images in supine position were significantly correlated with those obtained from PFT ( $R^2 > 0.88$ ). Next, with the image at FRC, we calculated air-trapping percentages (AirT%) for all subjects (Table 2). There was no

significant difference of AirT% between healthy and non-severe subjects ( $P > 0.46$ ), whereas AirT% was considerably elevated in the severe asthmatic, being consistent with the increased RV and FRC of the subject (Table 1).

### 3.2. Total and lobar air volume and airflow

Air volumes from CT images at respective phases were significantly correlated with corresponding air volumes measured continuously by the turbine-based flow meter ( $R^2 > 0.97$ ) With the meter-measured air volumes, we estimated normalized total airflow ( $Q^*$ , Eq. 1) for all subjects. Figure 1 indicated  $Q^*$  as a function of  $V_{air}^*$  for healthy and asthmatic subjects. All subjects demonstrated similar trends during tidal breathing. However, the asthmatics had greater  $Q^*$  during exhalation ( $P < 0.05$ ) while the difference was not significant during inhalation ( $P > 0.15$ ).

We obtained the means of lobar air volume fraction,  $v_{f,air}$ , i.e. the ratio of lobar air volume to total air volume, for five non-severe asthmatics and one severe asthmatic (Figure 2). The trends of non-severe asthmatics (Figure 2, A and B) were similar with those of healthy subjects (Jahani et al., 2015) in that  $v_{f,air}$  of upper lobes decreased and  $v_{f,air}$  of lower lobes increased with increasing total lung volume ( $P < 0.05$ , between EE and EI). On the other hand, the severe asthmatic subject exhibited the opposite trends (Figure 2, C and D). Lobar flow fractions  $q_f$  (Eq. 7) for all subjects were then compared between static and dynamic scans in Figure 3. Linear interpolation was employed to calculate  $q_f$  for static scans between TLC and FRC ( $q_{f,SCT}$ ), and cubic interpolation was used to calculate  $q_f$  for dynamic scans between EE and EI ( $q_{f,4D-CT}$ ). The  $q_{f,SCT}$  values were in similar range for all subjects (Figure 3A). However, the  $q_{f,4D-CT}$  for the severe asthmatic subject showed different values in the left lower lobe (LLL), left upper lobe (LUL) and right upper lobe (RUL) as compared with those for healthy and non-severe asthmatic subjects (Figure 3B). Figure 3C indicated that there was a good correlation between lobar  $q_{f,SCT}$  and  $q_{f,4D-CT}$  for both healthy ( $R^2 = 0.84$ ) and non-severe asthmatic ( $R^2 = 0.90$ ) subjects. However, statistical test between healthy and non-severe asthmatic subjects did not show significant difference ( $P > 0.05$ ). Nonetheless, the severe asthmatic showed deviations from the identity line in three lobes.

### 3.3. Heterogeneity of regional ventilation

To quantify global and lobar heterogeneity for airflow, we calculated CVs of local air volume changes for static (FRC vs. TLC) and dynamic (EE vs. EI) scans (Table 3). Heterogeneity in dynamic images significantly increased as compared with that in static images for healthy and asthmatic subjects ( $P < 0.005$ ). In addition, heterogeneity of lower lobes in the severe asthmatic was much greater than that of upper lobes in dynamic images while this feature was not observed in static images. To demonstrate the difference in heterogeneity between dynamic and static images, Figure 4 displayed normalized histograms for the relative local air volume change, normalized by the average air volume change over the whole lung for two representative subjects. One was a healthy subject with FEV1/FVC = 0.81 and the other was a non-severe asthmatic with FEV1/FVC = 0.60. In the Figure, “Normalized Frequency” means the number of voxels counted for each value divided by the total number of voxels. Dynamic images showed more widespread distribution, signifying



greater variation in air volume change at local (image-voxel) scale although lobar airflow fractions at global scale for static and dynamic images were similar (see Figure 3).

### 3.4. Non-linearity and hysteresis of lung motion

The normalized anisotropic deformation index ( $ADI^*$ ) was used to quantify non-linearity and hysteresis of lung deformation. For both healthy and asthmatic subjects,  $ADI^*$  and non-linearity ( $\delta_{ADI^*}$ ) during inhalation were in a same range and greater than those of exhalation (Figure 5). However, during exhalation, the  $\delta_{ADI^*}$  values for asthmatics were greater than those of healthy subjects. Figure 6 shows the means of non-linearity and hysteresis of different phases in each lobe. Consistent with total lungs, in all lobes except RUL, the  $\delta_{ADI^*}$  values for asthmatic subjects during exhalation were greater than those of healthy subjects (Figure 6A,  $P < 0.05$ ). Furthermore, for both healthy and asthmatic lungs, the left lungs had greater  $\delta_{ADI^*}$  during exhalation (Figure 6A), while the right lungs had greater  $\delta_{ADI^*}$  during inhalation (Figure 6B,  $P < 0.05$ ). Furthermore, the lower lobes had greater  $\delta_{ADI^*}$  than the upper lobes for all subjects ( $P < 0.05$ ). Consequently, greater values of  $\delta_{ADI^*}$  in asthmatics during exhalation resulted in less global and lobar  $Hys_{ADI^*}$  (Figure 6C).  $Hys_{ADI^*}$  of asthmatics was less than that of healthy subjects in all regions.  $Hys_{ADI^*}$  of the right lungs was greater than that of the left lungs for all subjects.

## 4. Discussion

Using the unique dataset of dynamic 4D-CT images, we analyzed regional ventilation, heterogeneity and lung deformation for asthmatics including five non-severe asthmatics and one severe asthmatic. The results were compared with the previously published 4D-CT data of five healthy subjects (Jahani et al., 2015). We further compared the differences between the analyses based on dynamic and static images. A dual rolling-seal piston system (Fuld et al., 2012) was utilized to control tidal volume and reduce inter-subject variability (Figure 1). For analysis, we employed an image matching technique (Yin et al., 2009) to derive regional ventilation as well as metrics, such as ADI, to quantify non-linearity and hysteresis.

### 4.1. Regional ventilation

We first investigated air trapping (AirT%) at FRC scans, because it has been widely used as a putative index of small airways disease (Busacker et al., 2009; Choi et al., 2014; Newman et al., 1994). In the current study, AirT% in non-severe asthmatics was similar with that of healthy subjects (Table 2), implying that the baseline lung functions of non-severe asthmatic are close to normal lung. This was further supported by the fact that both healthy and non-severe asthmatic subjects showed similar trends of lobar air volume fraction during tidal breathing (Jahani et al., (2015) and Figure 2A and B). However, unlike the non-severe asthmatic and healthy subjects, the air volume fraction in upper lobes increased at larger lung volumes in the severe asthmatic (Figure 2C and D). This is possibly due to significant air trapping of the lower lobes (Table 2) as demonstrated by Choi et al., (2013) that air trapping predominantly occurs in the lower lobes of severe asthmatics.

Ventilation heterogeneity during tidal breathing was predominantly increased relative to those during deep breathing for both healthy and asthmatic subjects. However, there was no



significant difference of ventilation heterogeneity between healthy and non-severe asthmatic subjects. The increased heterogeneity in dynamic scans may be attributable to the presence and heterogeneous variation of airway resistance during breathing and the absence of resistance during breath-hold for static scans (Hasan, 2010). Similar characteristics of airway resistance between asthmatic and non-asthmatic lungs were also observed in study done by Wongviriyawong et al., (2013). In their study, at baseline, airway resistances for healthy and asthmatic subjects were similar, whereas greater resistance, as expected, was found in asthmatic lungs after methacholine challenge. Investigation of lobar ventilation heterogeneity also increased during dynamic breathing, but their quantities were different in each lobe. For example, the severe asthmatic exhibited higher heterogeneity especially in lower lobes. Furthermore, since lobar airflow fractions between static and dynamic scans were well correlated for both healthy and non-severe asthmatic subjects in lobar scale (Figure 3C), smaller regions such as constricted small airways might be responsible for different ventilation heterogeneity between dynamic and static images (Venegas et al., 2005).

Because of increased heterogeneity and airway resistance during tidal breathing, if asthmatics respond to some prevailing techniques (e.g. methacholine challenge), 4D-CT analysis can be combined with those techniques to assess ventilation heterogeneity. Physiologically, ventilation heterogeneity can be used to determine airway hyper-responsiveness in asthmatics and is a sensitive metric for asthmatic alteration (Downie et al., 2007). Thus, ventilation heterogeneity estimated from 4D-CT analysis could be utilized as a quantitative biomarker to determine asthma severity, airway hyper-responsiveness and response to the treatment.

In addition, several studies utilized SPECT/CT images to quantify regional ventilation, its heterogeneity and particle deposition during deep breathing (Conway et al., 2012; De Backer et al., 2010). Fleming et al. (2015) indicated that asthma would not change fraction of inhaled particles in the lungs, which is in agreement with our findings for air flow fraction (Figure 3). However, none of those studies have investigated ventilation during dynamic breathing. Although SPECT/CT provides good visualization of ventilation heterogeneity and enables evaluation of the distribution of particle depositions, there are limitations such as long acquisition time and irregular breathing pattern during dynamic breathing and the need for using radioactive tracer. De Backer et al., (2010) showed that there is a good correlation between air flow distributions and ventilation heterogeneity derived from quantification of a radioactive tracer distribution using SPECT/CT technique and the one through the combination of CT imaging and CFD simulation. Furthermore, over dynamic breathing, Fuld et al., (2008) demonstrated in a supine sheep that regional ventilation derived from a xenon-CT method is in good correlation with regional specific volume change extracted from CT image analysis. Therefore, CFD can be combined with 4D-CT images acquired during consistent dynamic breathing using the dual piston system to provide physiological boundary conditions to analyze air flow and particle deposition (Miyawaki et al., (2016a) and Miyawaki et al., (2016b)). The analysis could provide information to improve the efficacy of inhalation drug delivery in patients with chronic lung diseases such as asthma.

## 4.2. Non-linearity and hysteresis

Assessment of lung deformation illustrated larger non-linearity for all asthmatics (non-severe and severe: Figure 5) relative to healthy subjects during exhalation. Physiologically, airflow resistance due to airway narrowing would be elevated during exhalation as compared with that during inhalation, because transpulmonary pressure is negative during exhalation (Hughes and Black, 2011). Therefore, the respiratory system needs to provide higher forces and works to overcome the resistance during exhalation (Hughes and Black, 2011; Levitzky, 2013). Some of those forces, such as shear forces, are correlated with anisotropic deformation (Fung, 1965; Jahani et al., 2014). Thus, we speculated that larger anisotropic deformation and nonlinearity of asthmatic lungs during exhalation were due in part to increased shear forces produced during exhalation. Furthermore, the characteristics in lungs showing the increase of non-linearity during exhalation were demonstrated in most regions of asthmatics as compared with healthy subjects. Thus, lower total and regional hysteresis during exhalation in asthma is due to the higher non-linearity of increased shear forces, relative to healthy subjects. Assessment of local deformation, forces and pressure distribution would explain their contribution on bronchoconstriction in certain airways of asthmatics. Knowing the regional information of abnormality would help utilizing more effective region-specific treatment.

## 5. Conclusions

In this study, we found two significant differences between healthy and asthmatic subjects (both non-severe and severe) during exhalation. First, the increased normalized airflow and the other was the increased anisotropic deformation in asthmatics. In addition to the metrics discussed here, there is a need to investigate the relationship of local lung mechanics with global alterations. Analysis of 4D-CT can provide actual regional airflow and physiologically consistent boundary condition for CFD simulation to be used to shed light on the underlying mechanics and estimate pressure distribution. Having airflow and pressure distribution would provide information to identify and predict regional airflow obstruction and airway resistance in asthmatics. Furthermore, CFD simulation can predict particle deposition and aerosol behaviors crucial for improvement of inhaler devices and the inhaled particles.

Increased ventilation heterogeneity during dynamic breathing was observed in both healthy and asthmatic subjects. Although, the one severe subject indicated greater heterogeneity rather than heterogeneity of non-severe subjects, there is only one severe asthmatic and a statistical statement is not possible. To define common characteristics among asthmatic and healthy populations, an analysis with more subjects is desirable in the future when CT technologies are advanced with increased resolutions, reduced cost and reduced radiation dose. Given the limited number of samples, we focused the analysis on regional differences (both voxel-wise and lobar-wise analysis) between healthy and asthmatic subjects, such as regional ventilation, non-linearity and hysteresis and expanded physiological discussions of the current findings along with existing literatures.

## Acknowledgments

This work was supported in part by NIH grants R01-HL094315, U01-HL114494, R01-HL112986, P30-ES005605, S10-RR024738 and S10-RR022421.

## References

- Amelon R, Cao K, Ding K, Christensen GE, Reinhardt JM, Raghavan ML. Three-dimensional characterization of regional lung deformation. *J Biomech.* 2011; 44:2489–2495. [PubMed: 21802086]
- Boldea V, Sharp GC, Jiang SB, Sarrut D. 4D-CT lung motion estimation with deformable registration: Quantification of motion nonlinearity and hysteresis. *Med Phys.* 2008; 35:1008–1018. [PubMed: 18404936]
- Busacker A, Newell J, John D, Keefe T, Hoffman EA, Granroth JC, Castro M, Fain S, Wenzel S. A multivariate analysis of risk factors for the air-trapping asthmatic phenotype as measured by quantitative ct analysis. *Chest.* 2009; 135:48–56. [PubMed: 18689585]
- Campana L, Kenyon J, Zhalehdoust-Sani S, Tzeng YS, Sun Y, Albert M, Lutchen KR. Probing airway conditions governing ventilation defects in asthma via hyperpolarized MRI image functional modeling. *J Appl Physiol.* 2009; 106:1293–1300. [PubMed: 19213937]
- Chae EJ, Seo JB, Lee J, Kim N, Goo HW, Lee HJ, Lee CW, Ra SW, Oh Y-M, Cho YS. Xenon Ventilation Imaging Using Dual-Energy Computed Tomography in Asthmatics: Initial Experience. *Invest Radiol.* 2010;1. [PubMed: 19996763]
- Chang AE, Matory YL, Dwyer AJ, Hill SC, Girton ME, Steinberg SM, Knop RH, Frank JA, Hyams D, Doppman JL. Magnetic resonance imaging versus computed tomography in the evaluation of soft tissue tumors of the extremities. *Ann Surg.* 1987; 205:340–348. [PubMed: 3032120]
- Choi S, Hoffman EA, Wenzel SE, Castro M, Fain SB, Jarjour NN, Schiebler ML, Chen K, Lin CL. Quantitative Assessment of Multiscale Structural and Functional Alterations in Asthmatic Populations. *J Appl Physiol.* 2015; 118:1286–1298. [PubMed: 25814641]
- Choi S, Hoffman EA, Wenzel SE, Castro M, Lin CL. Improved CT-based estimate of pulmonary gas trapping accounting for scanner and lung-volume variations in a multicenter asthmatic study. *J Appl Physiol.* 2014; 117:593–603. [PubMed: 25103972]
- Choi S, Hoffman EA, Wenzel SE, Tawhai MH, Yin Y, Castro M, Lin CL. Registration-based Assessment of Regional Lung Function via Volumetric CT Images of Normals vs. Severe Asthmatics *J Appl Physiol.* 2013; 115:730–742. [PubMed: 23743399]
- Conway J, Fleming J, Majoral C, Katz I, Perchet D, Peebles C, Tossici-Bolt L, Collier L, Caillibotte G, Pichelin M, Sauret-Jackson V, Martonen T, Apiou-Sbirlea G, Muellinger B, Kroneberg P, Gleske J, Scheuch G, Texereau J, Martin A, Montesantos S, Bennett M. Controlled, parametric, individualized, 2-D and 3-D imaging measurements of aerosol deposition in the respiratory tract of healthy human subjects for model validation. *J Aerosol Sci.* 2012; 52:1–17.
- De Backer JW, Vos WG, Vinchurkar SC, Claes R, Drollmann A, Wulfrank D, Parizel PM, Germonpré P, De Backer W. Validation of Computational Fluid Dynamics in CT-based Airway Models with SPECT/CT. *Radiology.* 2010; 257:854–862. [PubMed: 21084417]
- de Lange EE, Altes TA, Patrie JT, Gaare JD, Knake JJ, Mugler I, John P, Platts-Mills TA. Evaluation of asthma with hyperpolarized helium-3 mri\*: Correlation with clinical severity and spirometry. *Chest.* 2006; 130:1055–1062. [PubMed: 17035438]
- de Lange EE, Altes TA, Patrie JT, Parmar J, Brookeman JR, Mugler JP III, Platts-Mills TAE. The variability of regional airflow obstruction within the lungs of patients with asthma: Assessment with hyperpolarized helium-3 magnetic resonance imaging. *J Allergy Clin Immunol.* 2007; 119:1072–1078. [PubMed: 17353032]
- Downie SR, Salome CM, Verbanck S, Thompson B, Berend N, King GG. Ventilation heterogeneity is a major determinant of airway hyperresponsiveness in asthma, independent of airway inflammation. *Thorax.* 2007; 62:684–689. [PubMed: 17311839]
- Fleming J, Conway J, Majoral C, Katz I, Caillibotte G, Pichelin M, Montesantos S, Bennett M. Controlled, Parametric, Individualized, 2-D and 3-D Imaging Measurements of Aerosol

- Deposition in the Respiratory Tract of Asthmatic Human Subjects for Model Validation. *J Aerosol Med Pulm Drug Deliv.* 2015; 28:432–451. [PubMed: 25859710]
- Fuld MK, Easley RB, Saba OI, Chon D, Reinhardt JM, Hoffman EA, Simon BA. CT-measured regional specific volume change reflects regional ventilation in supine sheep. *J Appl Physiol.* 2008; 104:1177–1184. [PubMed: 18258804]
- Fuld MK, Grout RW, Guo J, Morgan JH, Hoffman EA. Systems for Lung Volume Standardization during Static and Dynamic MDCT-based Quantitative Assessment of Pulmonary Structure and Function. *Acad Radiol.* 2012; 19:930–940. [PubMed: 22555001]
- Fung, Y. *Foundations of solid mechanics.* Prentice Hall; 1965.
- Hankinson JL, Kawut SM, Shahar E, Smith LJ, Stukovsky KH, Barr RG. Performance of american thoracic society-recommended spirometry reference values in a multiethnic sample of adults: The multi-ethnic study of atherosclerosis (mesa) lung study. *Chest.* 2010; 137:138–145. [PubMed: 19741060]
- Hankinson JL, Odencrantz JR, Fedan KB. Spirometric Reference Values from a Sample of the General U.S. Population. *Am J Respir Crit Care Med.* 1999; 159:179–187. [PubMed: 9872837]
- Hasan, A. *Understanding Mechanical Ventilation: A Practical Handbook.* Springer Science & Business Media; 2010.
- Hughes, M., Black, R. *Advanced Respiratory Critical Care.* OUP; Oxford: 2011.
- Iyer KS, Grout RW, Zamba GK, Hoffman EA. Repeatability and Sample Size Assessment Associated with Computed Tomography-Based Lung Density Metrics. *Chronic Obstr Pulm Dis Miami Fla.* 2014; 1:97–104.
- Jahani N, Choi S, Choi J, Iyer K, Hoffman EA, Lin C-L. Assessment of Regional Ventilation and Deformation Using 4D-CT Imaging for Healthy Human Lungs during Tidal Breathing. *J Appl Physiol.* 2015 jap.00339.2015.
- Jahani N, Yin Y, Hoffman EA, Lin CL. Assessment of regional non-linear tissue deformation and air volume change of human lungs via image registration. *J Biomech.* 2014; 47:1626–1633. [PubMed: 24685127]
- King GG, Eberl S, Salome CM, Meikle SR, Woolcock AJ. Airway closure measured by a technegas bolus and SPECT. *Am J Respir Crit Care Med.* 1997; 155:682–688. [PubMed: 9032213]
- King GG, Harris B, Mahadev S. V/Q SPECT: Utility for Investigation of Pulmonary Physiology. *Semin Nucl Med, SPECT V/Q Imaging of the Lungs.* 2010; 40:467–473.
- Levitzky, MG. *Pulmonary physiology.* 8. McGraw-Hill; New York: 2013.
- Miyawaki S, Choi S, Hoffman EA, Lin CL. A 4DCT imaging-based breathing lung model with relative hysteresis. *J Comput Phys.* 2016a; 326:76–90. [PubMed: 28260811]
- Miyawaki S, Hoffman EA, Lin CL. Effect of static vs. dynamic imaging on particle transport in CT-based numerical models of human central airways. *J Aerosol Sci.* 2016b; 100:129–139. [PubMed: 28090122]
- National Heart Lung and Blood Institute. Expert Panel Report 3 (EPR 3): guidelines for the diagnosis and management of asthma. Bethesda: National Institutes of Health; 2007.
- Newell JD, Fuld MK, Allmendinger T, Sieren JP, Chan KS, Guo J, Hoffman EA. Very Low-Dose (0.15 mGy) Chest CT Protocols Using the COPD Gene 2 Test Object and a Third-Generation Dual-Source CT Scanner With Corresponding Third-Generation Iterative Reconstruction Software. *Invest Radiol.* 2015; 50:40–45. [PubMed: 25198834]
- Newman KB, Lynch DA, Newman LS, Ellegood D, Newell J, John D. QUantitative computed tomography detects air trapping due to asthma. *Chest.* 1994; 106:105–109. [PubMed: 8020254]
- Reinhardt JM, Ding K, Cao K, Christensen GE, Hoffman EA, Bodas SV. Registration-based estimates of local lung tissue expansion compared to xenon CT measures of specific ventilation. *Med Image Anal.* 2008; 12:752–763. [PubMed: 18501665]
- Stocks J, Quanjer PH. Reference values for residual volume, functional residual capacity and total lung capacity. *ATS Workshop on Lung Volume Measurements Official Statement of The European Respiratory Society.* *Eur Respir J.* 1995; 8:492–506. [PubMed: 7789503]
- Venegas JG, Winkler T, Musch G, Vidal Melo MF, Layfield D, Tgavalekos N, Fischman AJ, Callahan RJ, Bellani G, Scott Harris R. Self-organized patchiness in asthma as a prelude to catastrophic shifts. *Nature.* 2005; 434:777–782. [PubMed: 15772676]

- White B, Zhao T, Lamb J, Wuenschel S, Bradley J, Naqa IE, Low D. Distribution of lung tissue hysteresis during free breathing. *Med Phys*. 2013; 40:43501.
- Wongviriyawong C, Harris RS, Greenblatt E, Winkler T, Venegas JG. Peripheral resistance: a link between global airflow obstruction and regional ventilation distribution. *J Appl Physiol*. 2013; 114:504–514. [PubMed: 23123354]
- Yamamoto T, Kabus S, Klinder T, Lorenz C, von Berg J, Blaffert T, Loo BW, Keall PJ. Investigation of four-dimensional computed tomography-based pulmonary ventilation imaging in patients with emphysematous lung regions. *Phys Med Biol*. 2011; 56:2279–2298. [PubMed: 21411868]
- Yin Y, Choi J, Hoffman EA, Tawhai MH, Lin CL. A multiscale MDCT image-based breathing lung model with time-varying regional ventilation. *J Comput Phys*. 2013; 244:168–192. [PubMed: 23794749]
- Yin Y, Choi J, Hoffman EA, Tawhai MH, Lin CL. Simulation of pulmonary air flow with a subject-specific boundary condition. *J Biomech*. 2010; 43:2159–2163. [PubMed: 20483412]
- Yin Y, Hoffman EA, Lin CL. Mass preserving nonrigid registration of CT lung images using cubic B-spline. *Med Phys*. 2009; 36:4213–4222. [PubMed: 19810495]

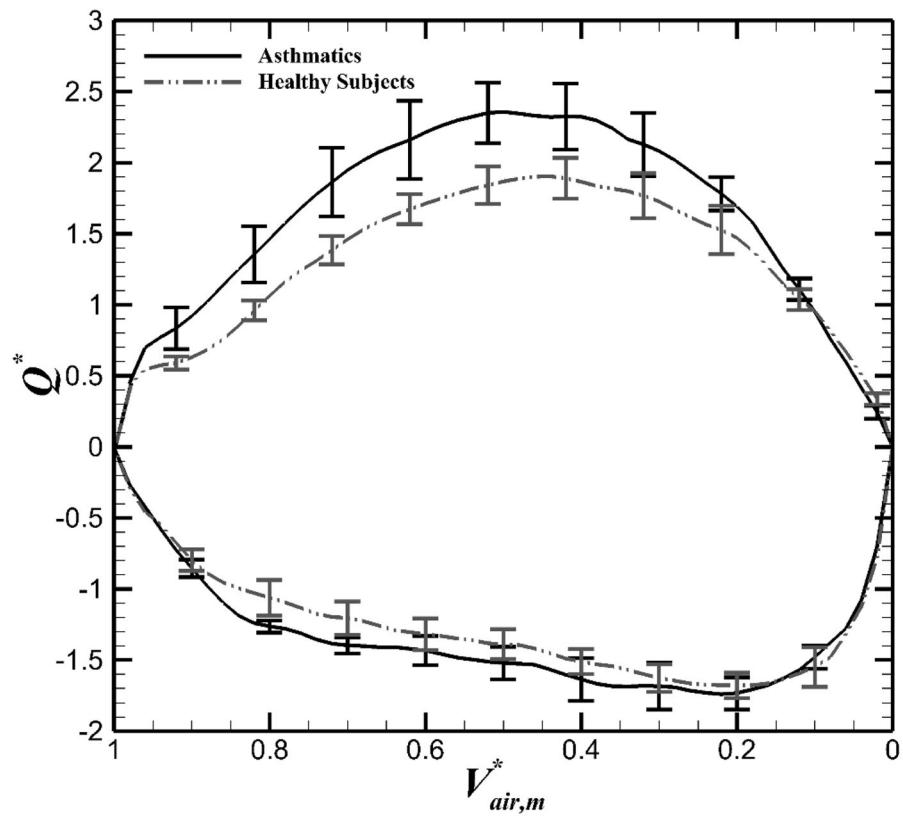


**Figure 1.** Means ( $\pm$ SE) of normalized airflow ( $Q^*$ ) measured by the turbine-based flow meter for exhalation (positive value) and inhalation (negative value) in the total lung for both asthmatic and healthy subjects.

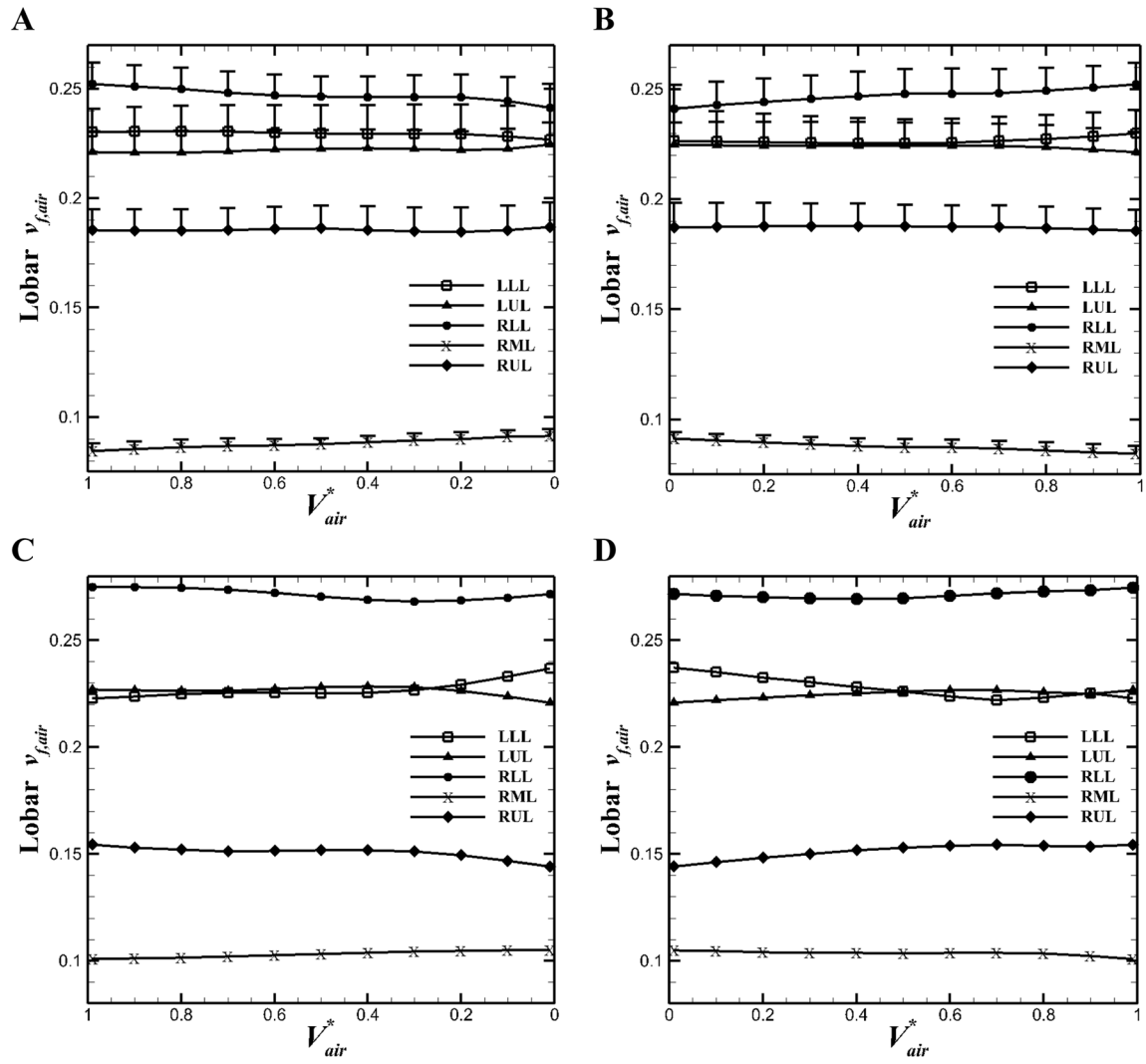


**Figure 2.** Means (+SE) of lobar air volume fraction for five non-severe asthmatics A: during exhalation and B: during inhalation, and for the severe asthmatic subject C: during exhalation and D: during inhalation.



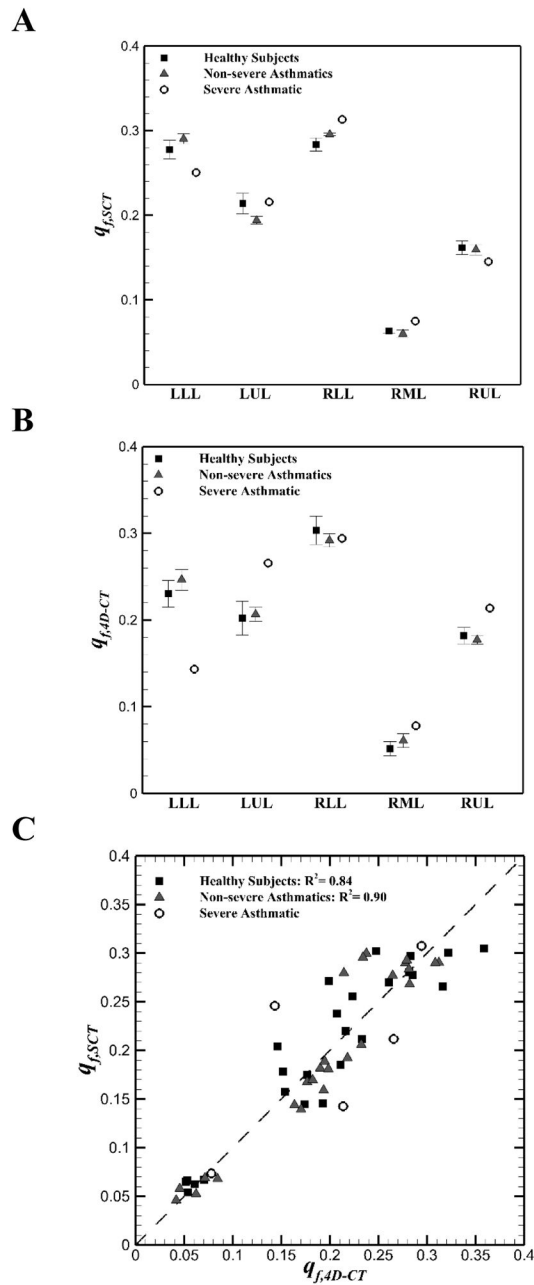


**Figure 3.** Means ( $\pm$ SE) of A: lobar airflow fraction ( $q_{f,SCT}$ ) in static scans, B: lobar airflow fraction ( $q_{f,4D-CT}$ ) in 4D-CT scans among healthy, non-severe asthmatic, and the severe asthmatic subjects; C: Comparison between lobar  $q_{f,SCT}$  and  $q_{f,4D-CT}$  for all subjects.

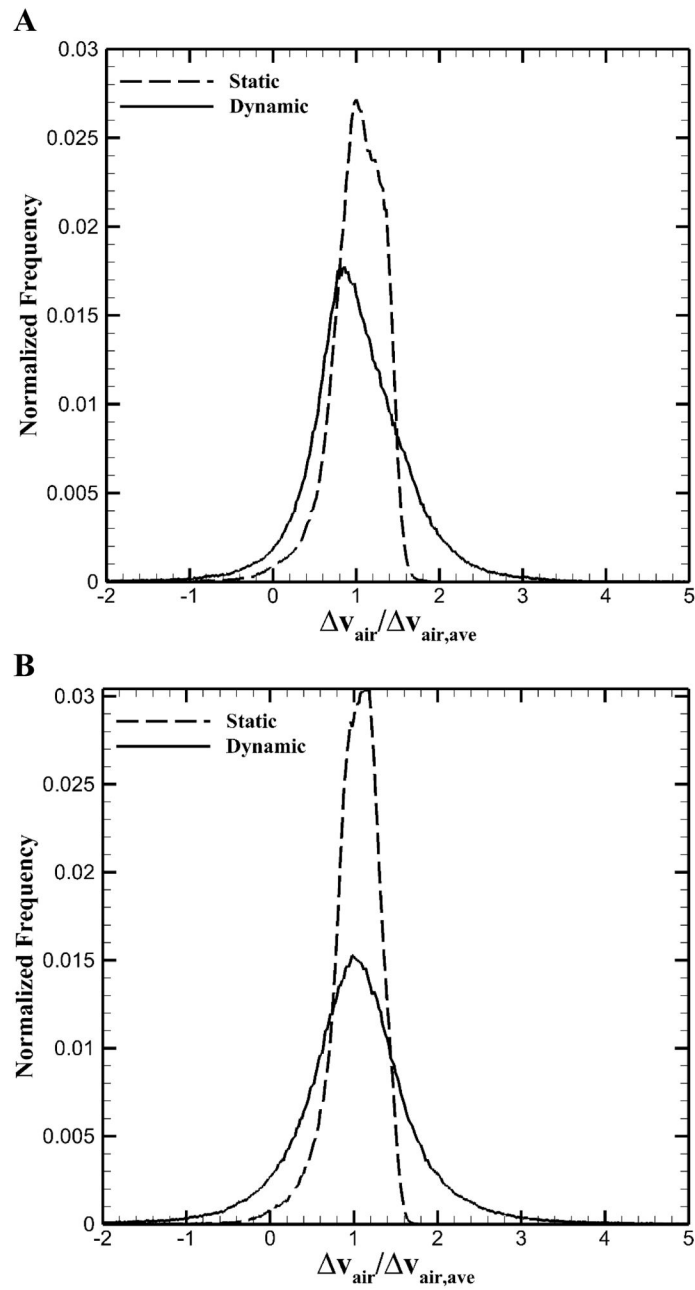


**Figure 4.** Voxel ventilation histogram for A: a representative healthy subject and B: a representative asthmatic subject.

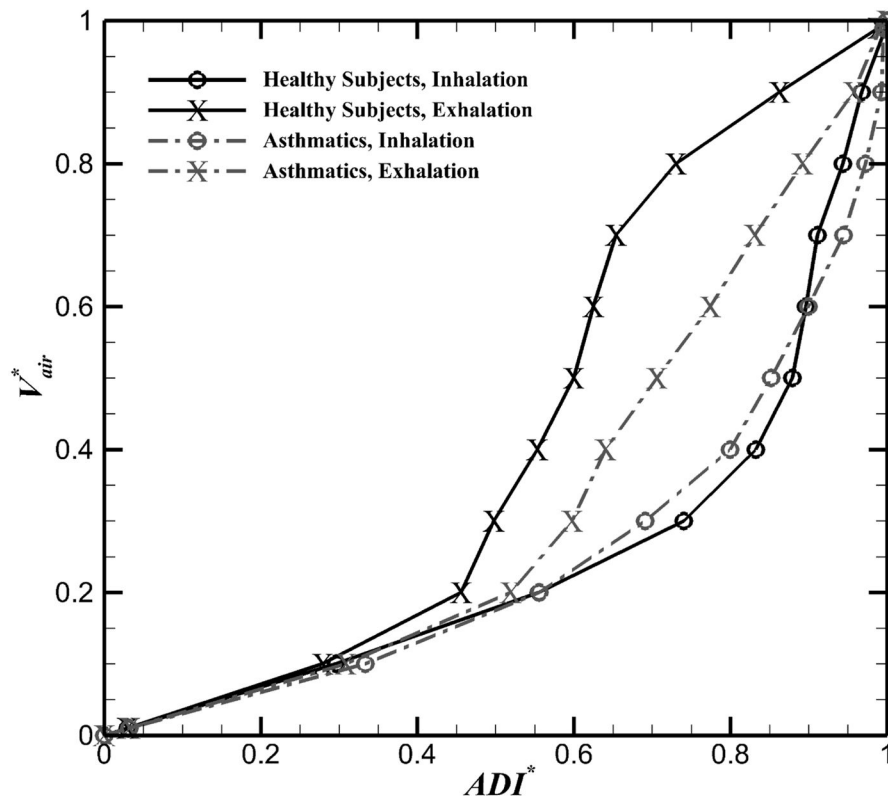


**Figure 5.** Means of ADI\* in the total lungs for five healthy and six asthmatic subjects.

Author Manuscript

Author Manuscript

Author Manuscript

Author Manuscript

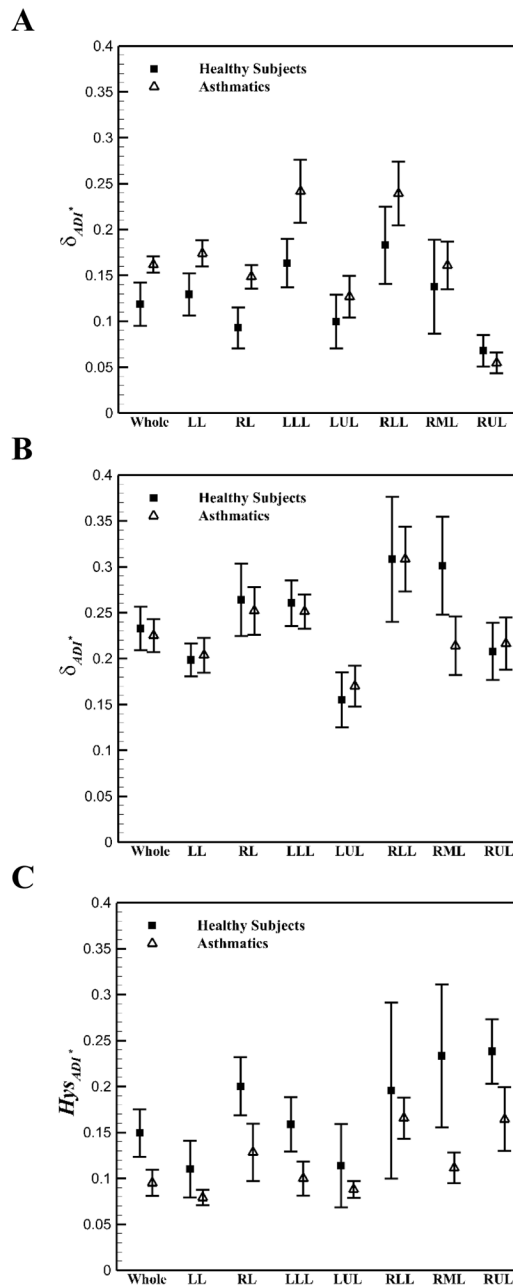


**Figure 6.** Means ( $\pm$ SE) of lung and lobar A: non-linearity of ADI\* during exhalation B: nonlinearity of ADI\* during inhalation, and C: hysteresis of ADI\* between five healthy and six asthmatic subjects.

**Table 1**

Demographic and PFT information for five healthy, five non-severe asthmatic and one severe asthmatic subjects

	Healthy	Non-severe asthmatic	Severe asthmatic	Mann-Whitney U test <sup>†</sup> ( <i>P</i> value)
Subjects, <i>n</i> (female)	5 (2)	5 (2)	1 (1)	
Age, <i>yr</i>	40 ± 15	37 ± 13	52	0.89
BMI, kg/m <sup>2</sup>	27 ± 3	26 ± 5	31	0.91
Race, <i>n</i> (white non- Hispanic/Hispanic/Asian)	4 / 1 / 0	5 / 0 / 0	0 / 0 / 1	-
TLC, %predicted	94 ± 7	95 ± 7	99	0.92
FRC, %predicted	82 ± 10	95 ± 16	128	0.12
RV, %predicted	83 ± 12	89 ± 6	153	0.76
FVC, %predicted	94 ± 9	92 ± 9	72	0.75
FEV1, %predicted	92 ± 6	76 ± 7	36	< 0.05
FEV1/FVC × 100	79 ± 2	67 ± 5	39	< 0.01

Values are means ±SD; *n*, no. of subjects.

<sup>†</sup>Statistical tests were performed between five healthy and five non-severe asthmatic subjects.

**Table 2**

Means  $\pm$  SD of total and lobar AirT% at FRC for 5 healthy, 5 non-severe asthmatic, and 1 severe asthmatic subjects

	Healthy subjects	Non-severe asthmatics	Severe asthmatic	Mann-Whitney U test <sup>†</sup> (P value)
Total	9.1% $\pm$ 7.6%	6.1% $\pm$ 4.3%	51.3%	0.60
LLL	1.5% $\pm$ 1.1%	1.3% $\pm$ 0.5%	62.7%	0.75
LUL	10.7 $\pm$ 9.9%	6.7% $\pm$ 4.3%	42.1%	0.74
RLL	1.1% $\pm$ 0.7%	1.8% $\pm$ 2.1%	54.3%	0.75
RML	27.4% $\pm$ 20.2%	24.2% $\pm$ 16.4%	66.6%	0.92
RUL	9.3% $\pm$ 8.4%	6.4% $\pm$ 6.9%	30.3%	0.46

<sup>†</sup>Statistical tests were performed between five healthy and five non-severe asthmatic subjects.

**Table 3**

Means  $\pm$  SD of Coefficient of Variations of whole and lobar air volume change for healthy and asthmatic subjects during deep and tidal breathing.

	Healthy subjects		Non-severe asthmatics		Severe asthmatic		Mann-Whitney U test <sup>†</sup> (P value)
	CV <sub>static</sub>	CV <sub>dynamic</sub>	CV <sub>static</sub>	CV <sub>dynamic</sub>	CV <sub>static</sub>	CV <sub>dynamic</sub>	
Whole	0.31 $\pm$ 0.03	0.79 $\pm$ 0.29	0.29 $\pm$ 0.02	0.68 $\pm$ 0.18	0.413652	0.934951	<0.005
LLL	0.22 $\pm$ 0.02	0.73 $\pm$ 0.19	0.22 $\pm$ 0.01	0.65 $\pm$ 0.20	0.412511	1.78656	<0.005
LUL	0.27 $\pm$ 0.05	0.80 $\pm$ 0.36	0.27 $\pm$ 0.02	0.63 $\pm$ 0.25	0.40323	0.62237	<0.005
RLL	0.23 $\pm$ 0.02	0.61 $\pm$ 0.21	0.23 $\pm$ 0.02	0.61 $\pm$ 0.15	0.370018	0.932261	<0.005
RML	0.49 $\pm$ 0.15	2.4 $\pm$ 3.04	0.43 $\pm$ 0.16	1.11 $\pm$ 0.39	0.534224	0.972335	<0.005
RUL	0.26 $\pm$ 0.02	0.59 $\pm$ 0.19	0.25 $\pm$ 0.02	0.55 $\pm$ 0.14	0.332232	0.398269	<0.005

CV<sub>static</sub>: Coefficient of Variation during deep breathing; CV<sub>dynamic</sub>: Coefficient of Variation during tidal breathing;

<sup>†</sup> Statistical tests were performed between CV<sub>static</sub> and CV<sub>dynamic</sub> for both healthy and non-severe asthmatic subjects.